MULTISCIA
JOURNALS PUBLISHERS

FRONTIERS IN PHARMACEUTICAL ANALYSIS

ISSN: (3065- 1352)

https://multisciajournals.com/journals/index.php/fpa
editor.fpa1@gmail.com

Frontiers in Zoological Research
Volume 1 Issue 3 2025

Dwarf surf clam (Mulinia lateralis) epigenetic regulation and maternal-to-zygotic transition: insights from transcriptomics and chromatin state profiling

A Naveen
Department of **Zoological Research**

Article Info

Received: 30-7-2025 Revised:08-09-2025 Accepted:19-09-2025 Published:29-09-2025

ABSTRACT

The group of Mollusca known as bivalve mollusks is important both taxonomically and commercially. Nevertheless, little is known about the regulatory processes controlling their embryonic growth. Recently, the dwarf surf clam (Mulinia lateralis) has been recognized as an appropriate model system for bivalve embryological study due to its high fertility and short generation period. By combining transcriptome analysis and chromatin-state profiling, this study investigated the epigenetic processes governing embryogenesis in M. lateralis, with an emphasis on the maternal-to-zygotic transition (MZT). High-resolution landscapes of the histone modifications H3K4me1, H3K4me3, H3K27me3, and H3K27ac throughout important developmental stages were created for the first time in this species using CUT&Tag. Significant histone mark reprogramming was found in the resultant data, suggesting dynamic changes in chromatin architecture throughout the early stages of embryonic development. The timing of MZT in M. lateralis between the morula and gastrula stages was determined by integration with transcriptome data, which also revealed a number of potential genes that are crucial for development. With implications for functional gene study and aquaculture progress, these findings establish M. lateralis as a reliable platform for epigenomic research in marine invertebrates and offer mechanistic insight into chromatin-mediated control of bivalve embryogenesis.

Keywords: CUT&Tag, Mulinia lateralis, epigenetic control, histone alterations, maternal-to-The zygotic transition

OVERVIEW

In eukaryotes, chromatin organization is controlled by the architecture of nucleosomes, which allows for dynamic regulation of gene expression and effective DNA packaging. DNA methylation, histone post-translational changes, and chromatin remodeling are examples of epigenetic mechanisms that coordinate this regulatory plasticity (Eichten et al., 2014; Turner, 2007). These alterations, which mainly affect chromatin accessibility and structure, regulate gene expression without changing the DNA sequence (Eichten et al., 2014). Histone alterations are a particularly intricate and instructive layer of epigenetic control among them. Histone tails act as dynamic platforms for the recruitment of regulatory proteins and remodeling complexes through chemical changes like methylation, acetylation, and phosphorylation, which shapes transcriptional outcomes (Bannister & Kouzarides, 2011; Millán-Zambrano et al., 2022; Turner, 2007). Many histone modifications have been found, and some of them are important indicators of cis-regulatory elements and chromatin states, especially in non-coding genomic areas (Millán-Zambrano et al., 2022). While H3K4me1 and H3K27ac are mostly linked to active enhancers and H3K27me3 is associated with repressive

chromatin areas, H3K4me3 is usually enriched at actively transcribing promoters (Blayney et al., 2023; Millán-Zambrano et al., 2022). In addition to defining the functional arrangement of chromatin, these epigenetic fingerprints make it possible to identify regulatory components that affect gene expression, such as promoters and distal enhancers in

Accepted: July 21, 2025; Received: May 29, 2025; Online: July 22, 2025

Foundation items: Shandong Provincial Special Funds for Taishan Scholars (tsqn202306104), Hainan Province "South China Sea New Star" Science and Technology Innovation Talent Platform Project (NHXXRCXM202365), Hainan Provincial Joint Project of Sanya Yazhou Bay Science and Technology City Grant (2021JJLH0090), and the National Natural Science Foundation of China (32200667) provided funding for this work.

domains that do not code (Blayney et al., 2023). Deciphering the intricate transcriptional networks that propel embryonic development requires an understanding of these chromatin-based regulatory processes. Histone alterations have important roles in the precise control of genes throughout embryogenesis, which is crucial for directing the creation of cell identity and organismal architecture (Bannister & Kouzarides, 2011; Schulz & Harrison, 2019; Turner, 2007). Maternally inherited mRNAs and proteins primarily control gene expression in the early stages of embryonic development. Maternal-to-zygotic transition (MZT) is a crucial developmental milestone that involves extensive genome remodeling and epigenetic reconfiguration to ensure proper expression patterns for cell fate determination (Schulz & Harrison, 2019; Xia et al., 2019). As development advances, transcriptional control shifts to the embryonic genome. In model organisms like Drosophila, zebrafish, and mice, the timing, regulatory architecture, and molecular basis of the MZT have been thoroughly studied (Sotomayor-Lugo et al., 2024; Vastenhouw et al., 2019); however, they show notable interspecies variability that is inconsistent with evolutionary relatedness (Fukushima et al., 2023; Vastenhouw et al., 2019). Humans, mice, zebrafish, Xenopus, Drosophila, and Caenorhabditis elegans have all been shown to exhibit distinct global patterns of histone modifications prior to and during zygotic genome activation (ZGA). These findings underscore the evolutionary flexibility of chromatin regulation during the early stages of embryogenesis (Lindeman et al., 2011; Millán-Zambrano et al., 2022; Vastenhouw et al., 2019; Xu et al., 2021).

Despite its significance, little is known about the regulatory dynamics of the MZT in bivalves, a complex and evolutionarily unique class of Mollusca known for its morphological diversity and specific life cycle strategies. An essential model system for researching the ontogeny of marine invertebrates, bivalve development follows a biphasic trajectory, with pelagic larval stages giving way to sessile benthic adults (Wang et al., 2020). Nevertheless, little is known about the molecular processes controlling bivalves' development, especially those pertaining to epigenetic regulation. The trochophore stage is a crucial and evolutionarily conserved larval form seen in many marine taxa, and bivalves generally undergo an indirect developmental phase. Specialized morphogenetic mechanisms and functional adaptations necessary for larval survival and dispersal define this stage (Wang et al., 2020). In contrast to the regulative development seen in other taxa, bivalves, being protostomes, display mosaic development characterized by spiral cleavage and deterministic cell fate specification, wherein embryonic fates are set early and stay fixed (Drozdov et al., 2023). Apart from their biological importance, bivalves account for more than 20% of the world's aquaculture production (FAO, 2024). Taxa like clams, mussels, scallops, and oysters are high-

yield protein sources that are distinguished by their quick growth, prodigious reproduction, and wide tolerance to a variety of environmental conditions (Vaughn & Hoellein, 2018). In addition to advancing our knowledge of their intricate regulatory networks, analyzing the epigenetic mechanisms—specifically, histone modifications—that govern their embryogenesis will offer a theoretical foundation for strengthening breeding tactics, boosting environmental resilience, and improving larval survival. Therefore,

Mechanistic insights and practical advantages in developmental biology and marine biotechnology could result from the advancement of epigenetic studies in bivalves. Because of its short generation period and translucent larval stages that allow for high-resolution imaging and experimental manipulation, Mulinia lateralis has become a potent model for bivalve developmental investigations (Yang et al., 2021). Cleavage Under Targets & Tagmentation (CUT&Tag) was used to create genome-wide profiles of important histone modifications (H3K4me1, H3K4me3, H3K27me3, and H3K27ac) across developmental stages in order to study the epigenetic mechanisms directing early embryogenesis in this species. To find possible regulatory genes that could drive embryonic development, these chromatin maps were combined with transcriptome information. An affordable and scalable substitute for conventional ChIP-seq in chromatin profiling is CUT&Tag, a highly sensitive technique with little input material (Kaya-Okur et al., 2019, 2020). With an emphasis on the MZT, a crucial window of regulatory reprogramming, our study sought to develop a thorough epigenomic landscape of M. lateralis embryogenesis. It was proposed that chromatin state transitions that regulate embryonic genes are correlated with temporally dynamic, stage-specific patterns of histone modification. It is anticipated that the results of this work will contribute to both practical applications in bivalve aquaculture and basic developmental biology.

SUPPLIES AND TECHNIQUES

Induction of spawning, fertilization, culture of larvae, and gathering of samples

The Ocean University of China's Laboratory of Marine Genetics and Breeding in Qingdao, China, provided the M. lateralis specimens used in this investigation. Animals were collected for this study without obtaining field authorization. Every experimental procedure detailed in this study was carried out in accordance with national, international, and institutional regulations.

In order to trigger spawning, sexually mature male and female animals were shade-dried for two hours before being moved to 500 mL crystallizing plates filled with sterile-filtered seawater (FSW) kept at 26–27°C with a salinity of 27–28 ppt (Yang et al., 2021). When sperm or egg release began, individuals were promptly removed, rinsed with FSW, and put in different culture dishes to continue gamete release. Spawning behavior was continuously observed. Gamete morphology was used to determine sex; eggs showed up at the bottom of the dish as yellow granular formations, while sperm showed up as white flocculent clumps. Eggs were filtered via a 150-mesh nylon screen stacked above a 500-mesh nylon screen to eliminate contaminants after being cleaned with FSW after gamete collection. Using a pipette, sperm was gathered and sent to a 50 mL centrifuge tube for further processing.

A 3:1 sperm-to-egg ratio was used for artificial fertilization. A 500-mesh nylon screen was used to filter out extra sperm after fertilization, and the fertilized eggs were then incubated in FSW at 21–22°C. At eight stages of development, samples were gathered: zygote (10 minutes after fertilization), 4-cell stage (1 hour after fertilization, hpf), D-shaped larvae (18 hpf), gastrula (6 hpf), blastula (4 hpf), morula (2 hpf), trochophore (10 hpf), and veliger stage (14 hpf). The gathered samples
were kept for later tests at -80°C after being flash-frozen in liquid nitrogen.

Data analysis and experimentation using CUT&Tag

Using previously established procedures, nuclei were isolated from flash-frozen samples (Kaya-Okur et al., 2019). With about 10,000 nuclei per sample, CUT&Tag libraries were created using

the Illumina Hyperactive Universal CUT&Tag Assay Kit (Vazyme, #TD903, China). Each developmental stage was represented by two biological duplicates. Supplementary Table S1 lists four histone mark-targeting antibodies (H3K4me1, H3K4me3, H3K27me3, and H3K27ac) as well as a non-specific IgG control. Since rabbit IgG (Abcam, ab172730, UK) does not recognize any specific histone modifications or chromatin-associated proteins, it was used as a negative control in conjunction with the histone mark-specific antibodies to evaluate the non-specific background signal. The dependability of the CUT&Tag peaks seen in the experimental samples was corroborated by the lack of signal enrichment in the IgG control, which confirmed the specificity of antibody binding (Kaya-Okur et al., 2019). Novogene (China) used the Illumina NovaSeq 6000 platform (USA) to sequence the produced CUT&Tag libraries.

The NGS QC Toolkit v.2.3 (Patel & Jain, 2012) was used to process raw sequencing data in order to produce clean, high-quality readings. Reads were aligned to the reference genome (unpublished) using BWA-MEM v.0.7.17 due to the structural complexity and repetitive content of the M. lateralis genome (Li, 2013). Duplicate BAM files were combined for further analysis after the resulting SAM files were filtered by fragment length using the awk tool. MACS2 v.2.2.7.1 (Feng et al., 2012) was used to identify peaks with the following parameters: macs2 callpeak -t IgG.bam -f A.bam -c BAMPE --outdir .../... - B -n A -g 1.44e9 --keep-dup auto -q 0.01. Supplementary Table S2 displays the mapping statistics.
Using the R packages GenomicFeatures (Lawrence et al., 2013), ChIPseeker (Yu et al., 2015), and ggplot2 (Wickham, 2011) in conjunction with Integrative Genomics Viewer (IGV) v.2.15.2, peak annotation and visualization were carried out. An established R pipeline (Kaya-Okur et al., 2019, 2020) was used to perform further analyses, such as peak signal enrichment heatmaps, fragment size distribution, repeatability of duplicate samples, and peak distribution across genomic regions (Figure 1).
Analysis of chromatin states
ChromHMM v.1.26 (Ernst & Kellis, 2017), which incorporates combinatorial histone modification patterns to infer chromatin states, was used to examine chromatin states across important embryonic stages in M. lateralis. Four histone modifications—H3K4me1, H3K4me3, H3K27me3, and H3K27ac—were used to train the model. The BinarizeBam module in ChromHMM was first used to binarize aligned BAM files with a 200 bp bin size and a 0.0001 signal detection P-value threshold. Ten different chromatin states were then inferred using a convergence threshold of 0.001 after the binarized data was trained using the LearnModel module. Lastly, IGV v.2.15 was used to annotate and visualize the genomic locations of the anticipated chromatin states. 2. Quantitative analysis and transmission electron microscopy (TEM)
First, the embryos were fixed for 24 hours in 2.5% glutaraldehyde.

After three rounds of washing in 1× phosphate-buffered saline (PBS), they were post-fixed for two hours at 4°C in 1% osmic acid. After that, the samples were gradually substituted with 90% acetone (HUSHI, China) after being successively dehydrated with 50%, 70%, and 90% ethanol. All of this was done at 4°C. To guarantee total dehydration, the samples were then subjected to three 15-minute treatments with 100% acetone at room temperature. After being immersed in epoxy resin (EPON 812, China), the dehydrated tissues underwent a 24-hour sequential polymerization process at 37°C, 45°C, and 60°C. An EM UC7 ultramicrotome (Leica, Germany) was used to create the ultrathin sections (70 nm), which were then stained with lead citrate and uranyl acetate and seen using a JEM-1200EX transmission electron microscope (JEOL, Japan).
Using ImageJ v1.54 and the Illumination Bias plugin (http://sites.imagej.net/Julien.pontabry/plugins/), a quantitative examination of nuclear ultrastructure was carried out in accordance with Laue et al. (2019). The maximum entropy thresholding approach was used to segment electron-dense versus non-electron-dense regions, and nuclear boundaries were manually drawn. Particles that were electron-dense and at least 0.03 μm2 in size were automatically chosen and counted. To create

standardized metrics for comparative analysis, the quantity and total area of electron-dense particles in each image were measured and normalized to the total nuclear area (Laue et al., 2019).

The use of immunofluorescence Overnight, embryos were preserved at 4°C in 4% paraformaldehyde (PFA). As outlined in other studies, immunofluorescence staining was carried out (Laue et al., 2019). PBST was used to wash fixed embryos, followed by three PBST washes and an overnight incubation period at 4°C with primary antibodies. After applying secondary antibodies and incubating them for the entire night at 4°C, three further PBST washes were performed. After 30 minutes of DAPI staining, three PBST washes were conducted before imaging under a fluorescence microscope.

The primary antibodies used in the CUT&Tag experiment were the same (Supplementary Table S1). Goat anti-rabbit immunoglobulin G (IgG) (Abcam, ab6702, UK) was conjugated with the Atto488 Conjugation Kit (Fast)-Lightning-Link® (Abcam, ab269896, UK) to create Atto488-conjugated secondary antibodies.

Transcriptomic analysis and RNA sequencing (RNA-seq) Three biological replicates of each of the eight developmental stages of M. lateralis were used for RNA-seq. The RNAprep Pure Tissue Kit DP431 (Tiangen, China) was used to extract total RNA, which was then processed with DNase I (Takara Bio, Japan) to eliminate genomic DNA. A Novue Plus spectrophotometer (GE Healthcare, USA) was used to measure the concentration and purity of the RNA, and agarose gel electrophoresis was used to verify the integrity of the RNA. The NEBNext® Ultra™ RNA Library Prep Kit for Illumina® (NEB, USA) was used to prepare the RNA libraries. Poly-T oligo-attached magnetic bead selection was used to enrich the mRNA and produce poly(A)+ RNA libraries. Novogene (China) sequenced libraries using the Illumina NovaSeq 6000 platform (USA), requiring 6 GB of raw data per sample. The NGS QC Toolkit v.2.3 (Patel & Jain, 2012) was used to quality filter raw readings in order to provide clean reads (Supplementary Table S3). STAR v.2.7.11b was used to match high-quality reads to the reference genome (Dobin et al.,

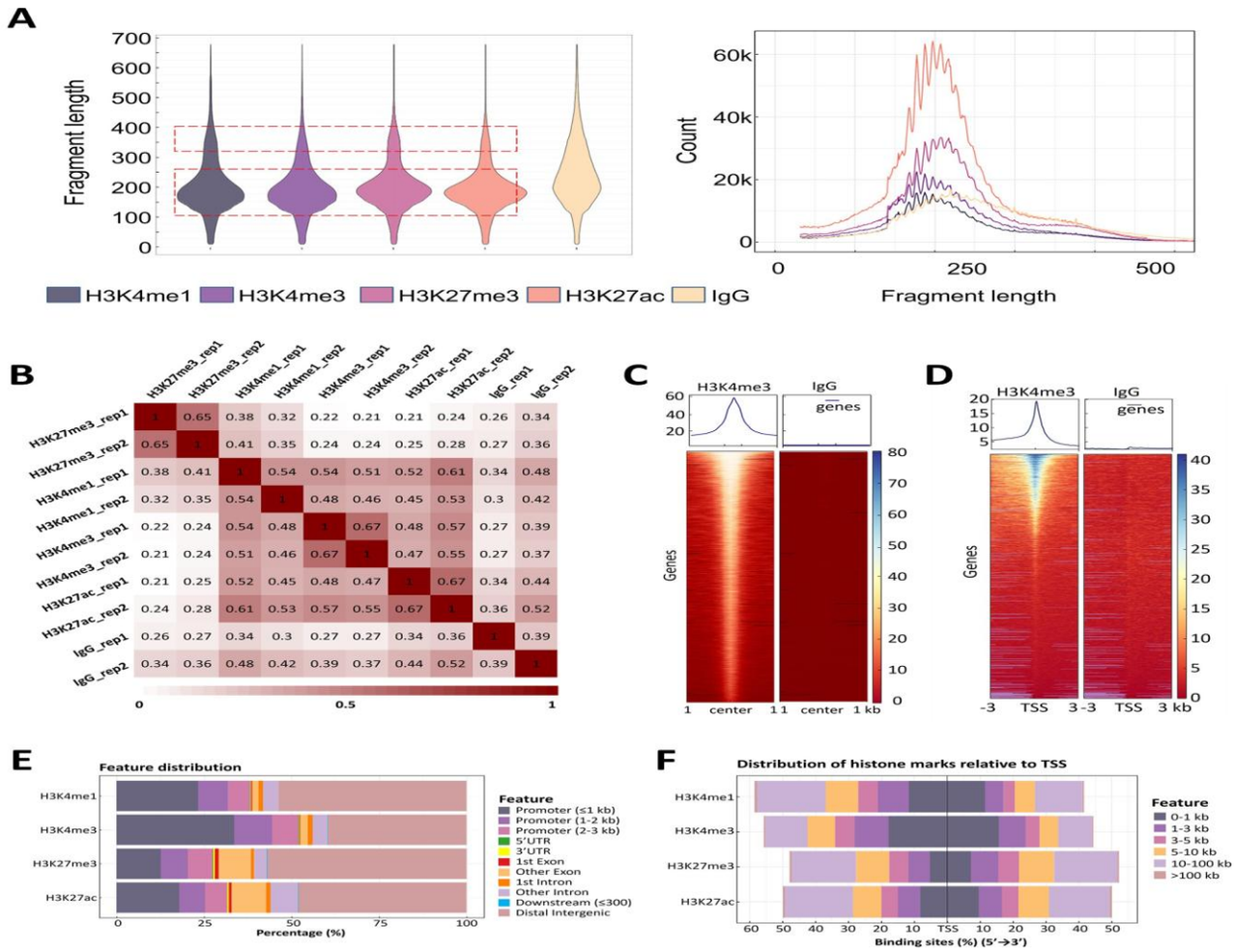

Figure 1 Quality assessment of CUT&Tag in *Mulinia lateralis* embryos at the trochophore stage

A: Distribution of fragment sizes: Plots displaying the number (right) and proportion (left) of DNA fragments by size. While control samples showed a random distribution, histone modification samples showed a high enrichment of mononucleosome-sized fragments. B: Replicate reproducibility: The reproducibility of CUT&Tag was confirmed by the high correlation found between duplicates of histone modification samples. C: Peak signal enrichment: Heatmaps (bottom) and plots (top) for histone modification (H3K4me3) and control (IgG) samples, respectively, displaying signal enrichment and random distribution within ±1 kb of the CUT&Tag peak. D: H3K4me3 enrichment at TSS: Plots (top) and heatmaps (bottom) demonstrate H3K4me3 enrichment close to TSS (±3 kb), while the IgG control sample showed no enrichment. E: Histone modification peak distribution among gene structural components. F: The ratio of histone modification peaks to the TSS by distance.

clustering and Spearman's correlation coefficients for pairwise similarity between biological replicates. Differential gene expression was analyzed using the DESeq2 package (Love et al., 2014) in Rstudio (v.4.2.1), with thresholds set at |Fold Change|>2 and a false discovery rate (FDR)-adjusted *P*-value<0.05. Functional enrichment of differentially expressed genes (DEGs) was conducted using Kyoto Encyclopedia of Genes and Genomes (KEGG) pathway analysis implemented in the clusterProfiler R package (Yu et al., 2012).

Weighted gene correlation network analysis (WGCNA) WGCNA was performed to identify modules of highly correlated genes across different developmental stages of *M. lateralis*. Genes with zero TPM in all samples were excluded to minimize noise from non-expressed genes. The WGCNA package in R (Langfelder & Horvath, 2008) was used to construct a gene co-expression network. Initially, hierarchical clustering (hclust) was applied to detect potential sample outliers. Soft-thresholding power was determined using the pickSoftThreshold function to establish scale-free topology (soft threshold=20).

An adjacency matrix was constructed to define gene co- expression relationships, and modules containing at least 800 genes were identified using the cutreeDynamic algorithm. Modules were visualized using Cytoscape (v.3.6.1), with the 30 most highly connected genes in each module highlighted in heatmaps. Functional annotation was performed using KEGG pathway enrichment via clusterProfiler in R (Yu et al., 2012), with significantly enriched pathways identified at *P*<0.05 (Supplementary Table S4).

Identification of EZH homologs, phylogenetic analysis, and multiple sequence alignment

To identify homologs of EZH1 and EZH2, protein sequences from various species, including *Homo sapiens*, *Mus musculus*, *Gallus gallus*, *Xenopus laevis*, *Xenopus tropicalis*, *Oryzias latipes*, *Danio rerio*, *Chionoecetes opilio*, *Amphibalanus Amphitrite*, *Drosophila melanogaster*, *Mytilus edulis*, *Mytilus galloprovincialis*, *Mizuhopecten yessoensis*, and *Patella vulgata*, were retrieved from the NCBI and Ensembl databases. Specific protein sequences and Accession IDs are provided in Supplementary Table S5.

Candidate EZH homologs in *M. lateralis* were identified by a BLAST search against the *M. lateralis* protein database, with an *E*-value threshold of <1E-5. Predicted homologous proteins were validated by detecting conserved domains using the SMART tool (https://smart.embl.de/) (Schultz et al., 1998). Phylogenetic analysis of the EZH1 and EZH2 protein sequences was conducted using the neighbor-joining method with 1 000 bootstrap

replicates. Multiple sequence alignments were conducted using Clustal W in MEGA v.11 (Tamura et al., 2021). The resulting phylogenetic tree was visualized using iTOL (https://itol.embl.de/) (Letunic & Bork, 2021).

Integrated analysis of CUT&Tag and transcriptome data H3K4me3 is a well-established marker of actively transcribed gene promoters, H3K27me3 is associated with polycomb repressive complex 2 (PRC2)-mediated silencing, and H3K27ac marks regions of open chromatin, particularly active enhancers when co-localized with H3K4me1 (Jiao & Liu, 2015; Zhu et al., 2023). To integrate CUT&Tag and transcriptome data, "bedtools intersect" (Quinlan, 2014) was used to identify genomic loci modified by specific histone marks. Genes were classified as actively transcribed if they met three criteria: average TPM≥1, presence of overlapping H3K27ac and H3K4me3 peaks (≥1 bp), and absence of H3K27me3 peaks within the promoter region, defined as a ±3 kb window centered on the transcription start site (TSS). This combinatorial chromatin signature reflects accessible promoter architecture conducive to active transcription, while the absence of H3K27me3 indicates a lack of polycomb-mediated repression. The TPM≥1 threshold was applied to eliminate low-abundance transcripts and ensure biological relevance. This integrative approach offers a more reliable and functionally meaningful classification of gene activity across developmental stages. KEGG pathway enrichment analysis was performed on these genes to identify significantly enriched pathways (P<0.05). Genes exhibiting at least 1 bp overlap between H3K4me1 and H3K27ac peaks, without H3K27me3 peak overlap, were defined as genes modified by active enhancer markers at specific developmental stages. Gene expression comparisons across stages were analyzed using GraphPad Prism v.8.0.2, and statistical differences were evaluated by two-tailed *t*-tests. Statistical significance was defined as: *: P<0.05; **: P<0.01; ***: P<0.001.

RESULTS

Establishment and validation of CUT&Tag in *M. lateralis* To optimize CUT&Tag for *M. lateralis*, two critical modifications were introduced to adapt the standard protocol to the biological and genomic characteristics of this species. First, nuclei were used instead of dissociated cells to overcome challenges associated with cell dissociation and to mitigate osmotic imbalances between marine invertebrate cells and standard buffers. This approach also reduced variability in cell-type representation across developmental stages caused by differential dissociation efficiency. Second, due to the high structural complexity and repeat content of the
M. lateralis genome, Bowtie2—originally recommended for CUT&Tag—yielded low alignment rates. In contrast, BWA- MEM, which offers greater tolerance for indels, repeats, and sequencing errors, exhibited substantially improved alignment performance, consistent with previous findings in complex genomes (Wu et al., 2019). Implementation of BWA-MEM increased mapping rates from approximately 50% to over 90% (Supplementary Table S2). Additionally, to address issues of multi-mapping in repeat-rich genomes, a common feature among marine invertebrates (Fallet et al., 2020), paired-end
150 bp (PE150) sequencing was employed to ensure sufficient read lengths for capturing 180 bp CUT&Tag fragments corresponding to single nucleosome-sized DNA.

CUT&Tag performance was validated by assessing alignment rates and fragment profiles. Most samples exhibited alignment rates exceeding 90%, with all samples achieving rates above 70%, indicating high mapping efficiency (Supplementary Table S2). Fragment size distribution revealed clear nucleosomal laddering in most histone-marked samples, whereas IgG controls lacked such patterns (Figure 1A; Supplementary Figure S1A), confirming

specific enrichment of histone modifications (Brahma & Henikoff, 2024; Ye et al., 2021). At the zygote stage, both mononucleosome and subnucleosomal fragments were detected, whereas no mononucleosome-sized fragments were observed at the 4-cell stage (Supplementary Figure S1A), potentially reflecting dynamic nucleosome reorganization during rapid cell divisions in early embryogenesis (Pecori &

Torres-Padilla, 2023; Wang et al., 2022).

Correlation analysis demonstrated moderate to high reproducibility across biological replicates. Moreover, the activating histone marks (H3K27ac, H3K4me1, and H3K4me3) exhibited stronger correlations among themselves than with either the IgG controls or repressive mark H3K27me3 (Figure 1B), supporting the specificity and consistency of the CUT&Tag profiles. These results are consistent with previous findings, particularly considering the higher cellular heterogeneity present in whole-embryo samples used in this study (Ye et al., 2021). Signal enrichment analysis revealed strong peak-centered signals for all four histone marks, while IgG controls exhibited no enrichment (Figure 1C), further validating peak specificity and reliability (Kaya-Okur et al., 2019).

Genome-wide distribution analysis revealed histone mark patterns consistent with those reported in other species (Boileau et al., 2023; Crespo et al., 2020; Pekowska et al., 2011; Pinello et al., 2014) (Supplementary Figure S1B). H3K4me3 was significantly enriched around TSS (Figure 1D), consistent with its canonical association with active promoters (Millán-Zambrano et al., 2022). Histone marks exhibited differential enrichment across genomic regions. At the trochophore stage, promoter-associated peaks accounted for 38% (H3K4me1), 52% (H3K4me3), 28% (H3K27me3), and
32% (H3K27ac), while peaks in distal intergenic regions accounted for 54%, 40%, 57%, and 48%, respectively. Peaks in untranslated regions (UTRs), exons, introns, and downstream regions contained comparatively fewer peaks (Figure 1E, F; Supplementary Figure S1B). These patterns indicate predominant localization of histone modifications in promoters and distal intergenic regions, highlighting their key regulatory roles. Notably, H3K27me3 remained stably distributed across genomic regions over the 6 developmental stages, while H3K4me1, H3K4me3, and H3K27ac exhibited pronounced redistribution between the morula and gastrula stages (Figure S1B), suggesting major chromatin remodeling and transcriptional activation events during this developmental window (Bae & Lesch, 2020; Yu et al., 2023).

Collectively, these results confirm the successful establishment and adaptation of CUT&Tag for *M. lateralis*, enabling robust profiling of histone modifications throughout embryogenesis. Given the conserved cellular and genomic features among marine invertebrates, this optimized protocol is likely to be broadly applicable across related taxa.

Chromatin state profiling during early embryogenesis in *M. lateralis*

Transcriptional regulation during embryonic development involves dynamic shifts in chromatin states that interact with trans-acting factors such as transcription factors. These chromatin states, defined by combinations of epigenetic modifications, not only reflect temporal changes in genome accessibility but also enable annotation of regulatory element and functional genomic regions across developmental stages (Ernst & Kellis, 2017; Liu et al., 2024). While individual histone marks provide valuable information about chromatin accessibility and transcriptional regulation, analyzing combinatorial patterns of multiple histone marks allows for a more comprehensive classification of chromatin states. These states correspond to distinct functional genomic elements, including promoters, enhancers, actively transcribed regions, and repressed domains, serving as a foundation forannotating functional elements in the *M. lateralis* genome.

To systematically define chromatin states in *M. lateralis*, ChromHMM, a computational tool for epigenomic annotation (Ernst & Kellis, 2017), was applied to genome-wide CUT&Tag profiles of four histone modifications—H3K4me1, H3K4me3, H3K27me3, and H3K27ac. Although chromatin state analyses are well established in vertebrate models, including mammals and fish, such approaches remain limited in bivalves (Fukushima et al., 2023; Rivera-Casas et al., 2017; Sotomayor-

Lugo et al., 2024; Zhu et al., 2019). To address this gap, chromatin state modeling was conducted in *M. lateralis* embryos to resolve the epigenomic landscape underlying early development.

Ten distinct chromatin states were inferred based on integration of the four histone modification marks, following standard ChromHMM protocols (Ernst & Kellis, 2017). These states were functionally interpreted based on histone mark combinations and genomic localization patterns (Ernst & Kellis, 2017; Roadmap Epigenomics Consortium et al., 2015), including: Active TSS (TssA), Flanking TSS (TssFlnk), Active Enhancer (EnhA1), Active Enhancer (EnhA2), Flanking Bivalent TSS/Enh (BivFlnk), Weak Flanking Bivalent TSS/Enh (BivFlnkWK), Repressed Polycomb (ReprPC), Weak Repressed Polycomb (ReprPCWk), Weak Transcription (TxWk), and Quiescent/low (Quies). TssA and TssFlnk, located near TSS, were both enriched for H3K4me3, with TssA also marked by H3K4me1 and H3K27ac, indicative of transcriptionally active promoters. EnhA1 and EnhA2 were enriched for H3K27ac, with EnhA1 showing higher H3K4me1 levels, consistent with active enhancer activity. Bivalent states co-enriched for active and repressive marks (e.g., H3K4me3/H3K27me3) may represent poised regulatory regions. ReprPC and ReprPCWk were defined by H3K27me3 enrichment, indicating polycomb-mediated repression. TxWk and Quies represented weakly transcribed or modification- depleted regions, respectively. It is important to note that ChromHMM state labels are based on probabilistic mark combinations and do not represent definitive functional assignments. For example, H3K4me1 may occur at both promoters and enhancers, and transitions between states (e.g., EnhA→TssFlnk→EnhA) may reflect dynamic regulatory element reuse rather than fixed functions. Interpretation of chromatin states should consider histone mark intensities, emission probabilities (Figure 2A), genomic annotations (Figure 2B), and gene expression profiles. The full chromatin state model captures the spectrum of transcriptional, enhancer, bivalent, repressive, and quiescent chromatin patterns and provides a genome-wide regulatory annotation for *M. lateralis* (Figure 2A–C).

To assess the biological relevance of the predicted chromatin states, the gene *sec61a* (FF-mul00016189) was examined as a representative locus. This gene encodes a conserved component of the SEC61 translocon complex, which facilitates co-translational protein transport into the endoplasmic reticulum and is involved in intracellular signaling (Bolar et al., 2016; Linxweiler et al., 2017). *Sec61a* exhibited significant up-regulation during the gastrula and trochophore stages, with corresponding chromatin states including TssFlnk, TssFlnkU, and enhancer-associated signatures enriched for H3K4me1 and H3K27ac. Visualization in IGV and gene expression analysis confirmed strong activation coinciding with predicted regulatory states (Figure 2D–E), supporting the functional relevance of the chromatin state

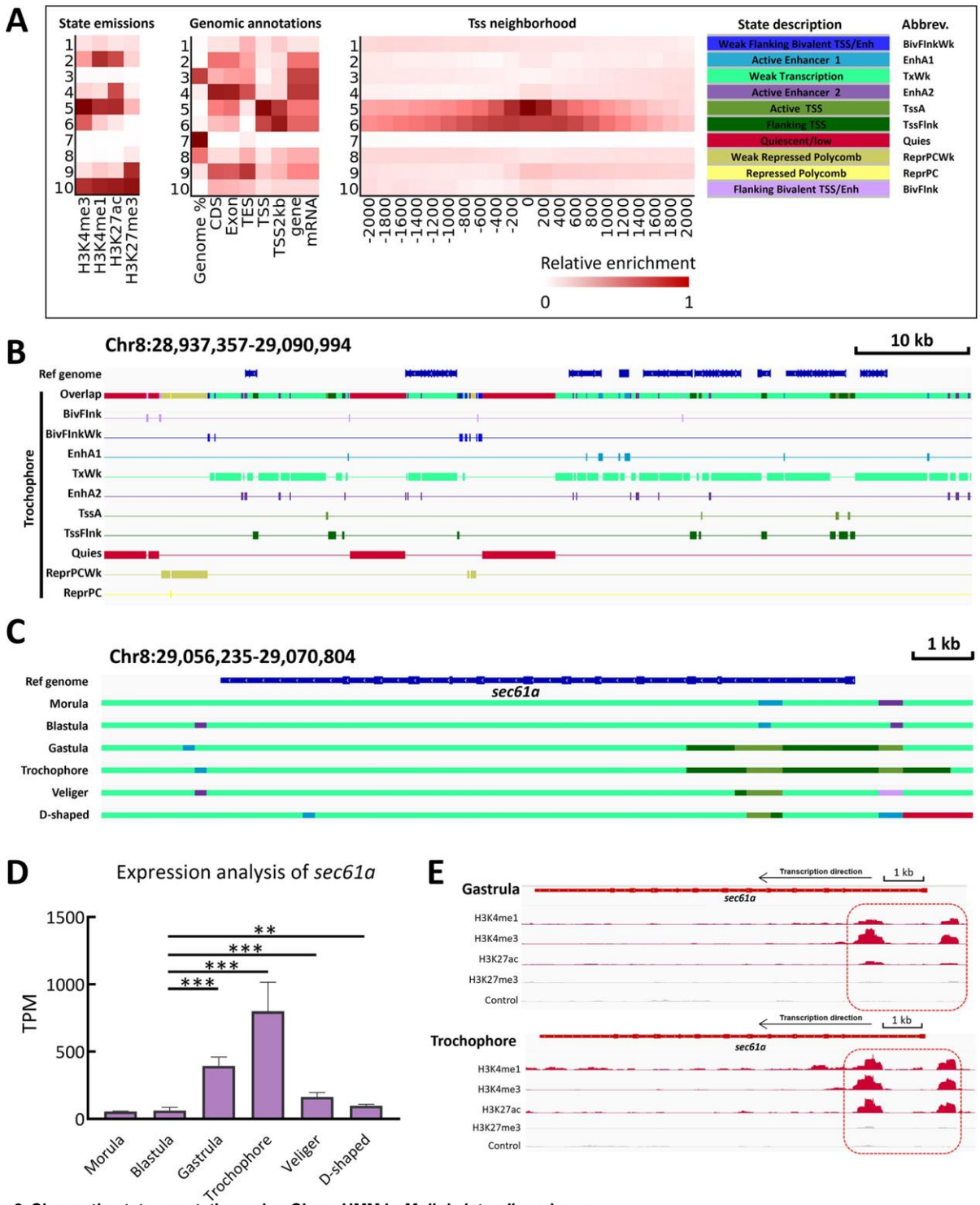

Figure 2 Chromatin state annotation using ChromHMM in *Mulinia lateralis* embryos

A: Chromatin states identified by chromHMM. Left panel: Heatmap of 10-state model emission parameters, with rows representing distinct chromatin states and columns representing histone marks. Color intensity represents probability of a given mark occurring in a particular state. Middle panel: Heatmap depicting enrichment of chromatin states at external genomic annotations, with color gradient reflecting degree of enrichment. Right panel: Heatmap illustrating enrichment of chromatin states within ±2 kb of TSS, with darker red indicating stronger enrichment and one color scale used for the entire heatmap. Candidate-state descriptions with abbreviations are listed on the right. B:

Genome browser view of chromatin states (cis-regulatory elements) identified by ChromHMM. Chromatin state tracks for trochophore stage are shown, with chromatin states displayed either in a compact format (all states combined) or individually (per state). C: Genome browser view of ChromHMM-based chromatin state annotations at the *sec61a* (FF-mul00016189) locus across six developmental stages of *M. lateralis* embryos. Each row represents a specific stage, and chromatin state colors are consistent across all panels. D: Expression levels of *sec61a* during *M. lateralis* embryonic development, quantified in transcripts per million (TPM). **: $P<0.01$; ***: $P<0.001$. E: IGV genome browser view displaying histone modification signal enrichment at the *sec61a* locus during the gastrula and trochophore stages, demonstrating correct chromatin state assignments as shown in C and confirming their association with transcriptional activity in D.

annotations. This chromatin state atlas provides a crucial reference for the functional genome annotation in *M. lateralis*. Integration with transcriptomic and epigenomic data offers insights into regulatory dynamics during embryogenesis and establishes a platform for comparative epigenomic analyses across marine invertebrates, contributing to a broader understanding of chromatin-mediated gene regulation in bivalves and evolutionary and developmental epigenomics. The complete chromatin state annotation dataset is available in the Supplementary File.

Histone modification dynamics and chromatin remodeling during early embryogenesis in *M. lateralis*

To elucidate histone modification dynamics during early embryonic development, genome-wide profiling of the four histone modifications was performed. Analysis of peak counts and the proportion of associated genes relative to the total annotated gene set revealed low abundance during early stages, followed by a substantial increase at the gastrula stage (Figure 3A). A corresponding rise in the proportion of genes associated with these marks was observed (Figure 3B), suggesting that histone modification remodeling occurs evenly across the genome rather than confined to specific loci. Among the four marks, H3K27me3 exhibited the earliest and broadest genomic distribution, with over 5 000 peaks corresponding to 14.65% of annotated genes at the morula stage (Figure 3A, B). This early enrichment of a repressive modification suggests the establishment of chromatin-based silencing before widespread ZGA, potentially restraining premature activation of developmental genes prior to lineage commitment (Lindeman et al., 2011; Xia et al., 2019). In contrast, permissive histone modifications such as H3K4me3, H3K4me1, and H3K27ac accumulated more gradually and reached wide prevalence at the gastrula stage (Figure 3A, B).

Given that deposition of H3K27me3 is catalyzed by PRC2 (Millán-Zambrano et al., 2022; Xia et al., 2019), transcript levels of its core components (EZH2, SUZ12, and EED) were examined to assess PRC2 activity during early chromatin regulation. Transcriptomic analysis revealed that *ezh2* (FF-mul00015448), encoding the PRC2 catalytic subunit, was highly expressed at the morula and blastula stages (Supplementary Figure S2A), supporting its role in early chromatin remodeling. Similarly, elevated transcript levels of *eed* (FF-mul00005678) and *suz12* (FF-mul00001742) at the morula stage (Supplementary Figure S2B, C) further support the functional activity of PRC2 during this period. The temporal correlation between increased PRC2 component expression and H3K27me3 accumulation further supports the potential role of PRC2 in mediating early chromatin repression at specific sites before widespread ZGA. Comparable mechanisms have been observed in zebrafish and mammals, where PRC2 activity is critical for

suppressing premature gene activation (Lindeman et al., 2011; Xia et al., 2019). Among these components, *EZH2* was identified as a key regulatory factor through integrated CUT&Tag and RNA-seq analysis (detailed in Section 3.6), which revealed its active zygotic transcription during the blastula stage (Figure 3C). To further examine its evolutionary conservation, phylogenetic and domain analyses were performed. In metazoans, two *EZH* genes—*EZH1* and *EZH2*—originated from a duplication event in a common ancestor of cartilaginous fish and bony vertebrates (Völkel et al., 2019). Unlike vertebrates, which possess both *EZH1* and *EZH2*, invertebrates possess only*EZH2* (Völkel et al., 2019). Consistent with this pattern, only a single *ezh2* gene was detected in the *M. lateralis* genome. Phylogenetic analysis positioned *M. lateralis* EZH2 within the molluscan clade, showing close evolutionary proximity to arthropod homologs and distinct separation from vertebrate EZH2 sequences (Supplementary Figure S2D). The domain structure of EZH2 in *M. lateralis* included conserved SANT, CXC, and SET domains, characteristic of functional histone methyltransferases (HMTases) (Supplementary Figure S2E). The SET domain, located at the C-terminus, contains the catalytic subunit responsible for H3K27 methylation (Sun et al., 2023). Comparative analysis of the SET domain revealed the substitution of amino acid residues Ile34 and Cys52 by Leu34 and Ser52 in EZH1 (Supplementary Figure S2F). These findings support the hypothesis that early repressive chromatin regulation in *M. lateralis* shares key evolutionary features with other metazoans but may also exhibit lineage-specific adaptations in bivalves. Future studies exploring PRC2-associated cofactors and regulatory mechanisms in mollusks may provide further insights into the evolutionary divergence of histone methylation pathways across invertebrates.

To provide ultrastructural validation of chromatin reorganization during early development, TEM was performed at key developmental stages (Laue et al., 2019). Consistent with histone modification profiles, dense chromatin aggregates were observed in nuclei at the blastula-stage and beyond, while such structures were sparse or absent during earlier stages (Figure 3D–G). These results suggest progressive compaction during development, aligning with the observed increase in repressive histone modification levels. Quantitative analyses of histone modification signal intensity and peak enrichment further supported this transition from an initially relaxed chromatin state to a more structured and repressed configuration (Figure 3H; Supplementary Figure S3A–D). The TEM results thus provide strong structural evidence for extensive chromatin remodeling during early embryogenesis.

The onset of widespread ZGA between the gastrula and trochophore stages was accompanied by a marked increase in permissive histone modifications, particularly H3K4me1, H3K4me3, and H3K27ac, consistent with their roles in enhancer and promoter activation (Millán-Zambrano et al., 2022). Transcriptomic profiling showed that *setd1b* (FF- mul00014078), one of the HMTases responsible for catalyzing H3K4 methylation and essential for embryogenesis and organogenesis—particularly during post-gastrula development (Kranz & Anastassiadis, 2020)—exhibited relatively stable mRNA levels throughout embryogenesis, while *wdr5* (FF- mul00021417) and *rbbp5* (FF-mul00018773), core scaffolding components of the H3K4 methyltransferase complex that facilitate catalytic activity (Hanna et al., 2022), showed increased expression from the gastrula stage (Supplementary Figure S3E–G). These findings suggest that the deposition of H3K4 methylation may be closely linked to the activation of zygotic transcription.

Dynamic transcriptomic and epigenetic reprogramming during MZT in *M. lateralis*

PCA of the transcriptomic data confirmed high reproducibility among biological replicates (Supplementary Figure S4A). Interestingly, samples from the eight developmental stages clustered into three distinct groups, indicating

distinct transcriptional shifts. The blastula and gastrula stages formed

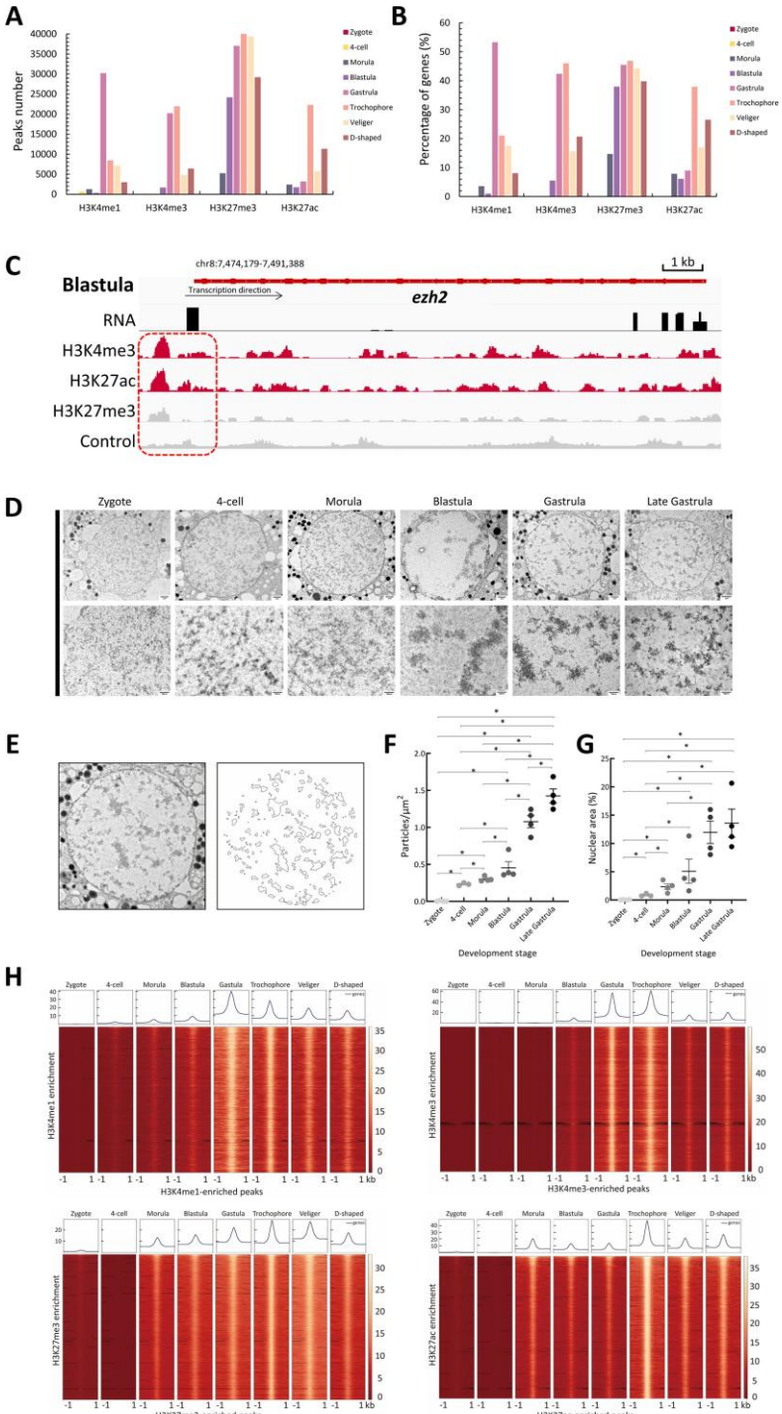

Figure 3 Histone modification dynamics during early embryonic development in *Mulinia lateralis*

A: Number of enriched peaks for H3K4me1, H3K4me3, H3K27me3, and H3K27ac across eight key developmental stages, illustrating dynamic chromatin landscape. B: Proportion of genes marked by each histone modification relative to the total number of genes in the genome at different developmental stages, reflecting progressive chromatin remodeling and transcriptional regulation. C: IGV view of *ezh2* expression and histone modification patterns at genomic loci during the blastula stage. Promoter region exhibits co-occurring H3K4me3 and H3K27ac peaks, indicative of active transcription, whereas H3K27me3 remains weakly enriched. D: Transmission electron micrographs of chromatin ultrastructure in embryonic cell nuclei at

different developmental stages. Higher magnification images highlight chromatin organization. Scale bars: 1 μm (nuclear images), 500 nm (high-magnification insets). E: Representative image illustrating electron-dense particle detection. F: Quantification of the number of particles per nuclear μm^2 in TEM images from zygote to late gastrula stage. G: Quantification of nuclear area (%) covered by particles in TEM images from the zygote to late gastrula stages. Nuclei from 3–4 embryos were analyzed per time point for electron-dense aggregate quantification. Each point represents data from one nucleus. *P*-values were calculated using Kruskal-Wallis tests (*: $P<0.05$), with error bars indicating standard deviation (SD). H: Heatmap of histone modification signal enrichment at all identified peak regions across eight key developmental stages. Signal intensities for H3K4me1, H3K4me3, H3K27me3, and H3K27ac are centered on peak summits and plotted within ±1 000 bp regions.

one cluster, while trochophore, veliger, and D-shaped larvae grouped together. In contrast, the zygote, 4-cell, and morula stages exhibited the most distinct gene expression patterns, likely reflecting the dominance of maternal mRNA during early development (Vastenhouw et al., 2019). Sample correlation analysis also demonstrated strong within-stage concordance among biological replicates, particularly among the early stages (Supplementary Figure S4B), further validating the stability and reproducibility of the data. Transcriptome profiling revealed that approximately 70% of annotated genes were expressed between the zygote and morula stages, consistent with patterns observed in *Drosophila melanogaster*, *Strongylocentrotus purpuratus*, and zebrafish (Vastenhouw et al., 2019). A sharp decline in RNA levels occurred at the blastula stage, suggesting large-scale maternal mRNA degradation between the morula and blastula stages. From the gastrula stage onward, gene detection gradually recovered and stabilized by the trochophore stage (Supplementary Figure S4C), indicating successful establishment of ZGA.

Maternal mRNA degradation may involve processing body (P-body)-mediated decay, as evidenced by the elevated expression of key P-body-associated genes *lsm14a* (FF-mul00010230) and *pdap1* (FF-mul00001599) during the blastula stage (Supplementary Figure S4D, E). LSM14A facilitates P-body formation and plays a major role in mRNA decay and storage (Brandmann et al., 2018; Stefano et al., 2019). PDAP1, a highly conserved P-body component, modulates *limd1* expression and contributes to P-body stability (Chirichella et al., 2022). Given that P-bodies function as hubs for post-translational regulation, the observed expression profiles suggest their involvement in maternal mRNA clearance during early embryogenesis (Beadle et al., 2023). However, direct evidence linking P-body activity to global maternal transcript degradation in *M. lateralis* remains to be established.

Histone modifications were also dynamically reprogrammed during embryogenesis, indicating coordinated epigenetic regulation of the MZT in *M. lateralis*. In the earliest stages (zygote to 4-cell), histone modifications were nearly undetectable, except for a few H3K4me1-marked loci (Figure 3A, B), and chromatin remained in a relatively relaxed state (Figure 3D). This transcriptionally permissive state supported maternal mRNA-driven development. By the morula stage, repressive histone mark H3K27me3 was already widespread, while permissive marks (H3K4me1 and H3K27ac) appeared at low abundance (Figure 3A, B). Early enrichment of the repressive mark likely contributed to transcriptional regression by preventing premature gene activation at selected sites. Concurrently, maternal mRNA degradation had commenced. During the blastula stage, maternal mRNA degradation peaked, RNA levels declined, and permissive H3K4me3

began to accumulate (Figures 3A, B, 5A; Supplementary Figure S4C), suggesting tight control of transcriptional activation. By the gastrula stage, ZGA was fully established, with widespread histone modifications, increased chromatin compaction, and transcriptional up-regulation (Figure 3A, B). These changes aligned with significant cellular differentiation events, suggesting that histone modifications may facilitate precise gene regulatory mechanisms during *M. lateralis* embryogenesis.

Collectively, these findings indicate that the MZT in *M. lateralis* occurs predominantly between the morula and gastrula stages, characterized by synchronized maternalmRNA transcript clearance and zygotic transcriptional activation (Figure 4). The coordinated regulation of histone modifications and transcriptional reprogramming provides a comprehensive molecular framework for understanding early embryonic regulation in bivalves and lay a foundation for future research into epigenetic regulation in marine invertebrate development.

Stage-specific gene expression dynamics and co- expression network architecture during *M. lateralis* embryogenesis

Integration of chromatin and transcriptomic profiling identified the MZT in *M. lateralis* as occurring between the morula and gastrula stages (Figure 4). To further resolve stage-specific transcriptional programs associated with zygotic genome activation, differential gene expression analysis was performed between consecutive developmental stages starting at the morula. KEGG enrichment analysis was subsequently applied to interpret functional associations of the identified DEGs. Marked transcriptomic reprogramming was observed, with significant up-regulation and down-regulation of mRNA levels across all stage transitions. Notably, the largest number of DEGs was detected between the blastula and morula stages, with 924 genes up-regulated and 5 029 genes down-regulated, consistent with widespread maternal mRNA degradation during this period. The observed increase in mRNA abundance at the blastula stage may, in part, reflect cytoplasmic polyadenylation of maternal mRNAs, a widely conserved mechanism across animal species during early embryogenesis (Subtelny et al., 2014). As embryonic development progressed, transcriptomic changes became more stage-specific, with 86, 384, 218, and 696 genes up- regulated at the gastrula, trochophore, veliger, and D-shaped larval stages, respectively (Figure 5A). These findings indicate a progressive establishment of zygotic transcriptional programs orchestrating stage-specific developmental processes in *M. lateralis*.

KEGG pathway enrichment analysis revealed dynamic functional reprogramming throughout development. During the blastula stage, DEGs were enriched in pathways associated with ribosome biogenesis, nucleocytoplasmic transport, and ErbB signaling, supporting rapid cell proliferation and division (Figure 5B). At the gastrula stage, DEGs were enriched in AMPK signaling and pluripotency-associated regulation, reflecting cell differentiation and germ layer formation. The trochophore and veliger stages were characterized by the up- regulation of genes involved in muscle development, immune response, and nervous system formation, including actin cytoskeleton regulation, leukocyte transendothelial migration, and Hippo signaling. By the D-shaped larval stage, genes related to energy metabolism and lipid biosynthesis pathways, such as cortisol synthesis and secretion, steroid hormone biosynthesis, and adipocytokine signaling, were up-regulated, corresponding to shell formation and larval development (Figure 5B). However, it is important to note that during early stages, particularly the blastula stage, functional analysis of DEGs based on RNA-seq data should be interpreted with caution due to the substantial influence of maternal RNAs.

To delineate transcriptional modules underlying coordinated gene expression, WGCNA was performed, grouping genes into

eight co-expression modules (M1–M8) with distinct temporal expression patterns (Figure 6A, B). Each module exhibited stage-specific activation and enrichment in

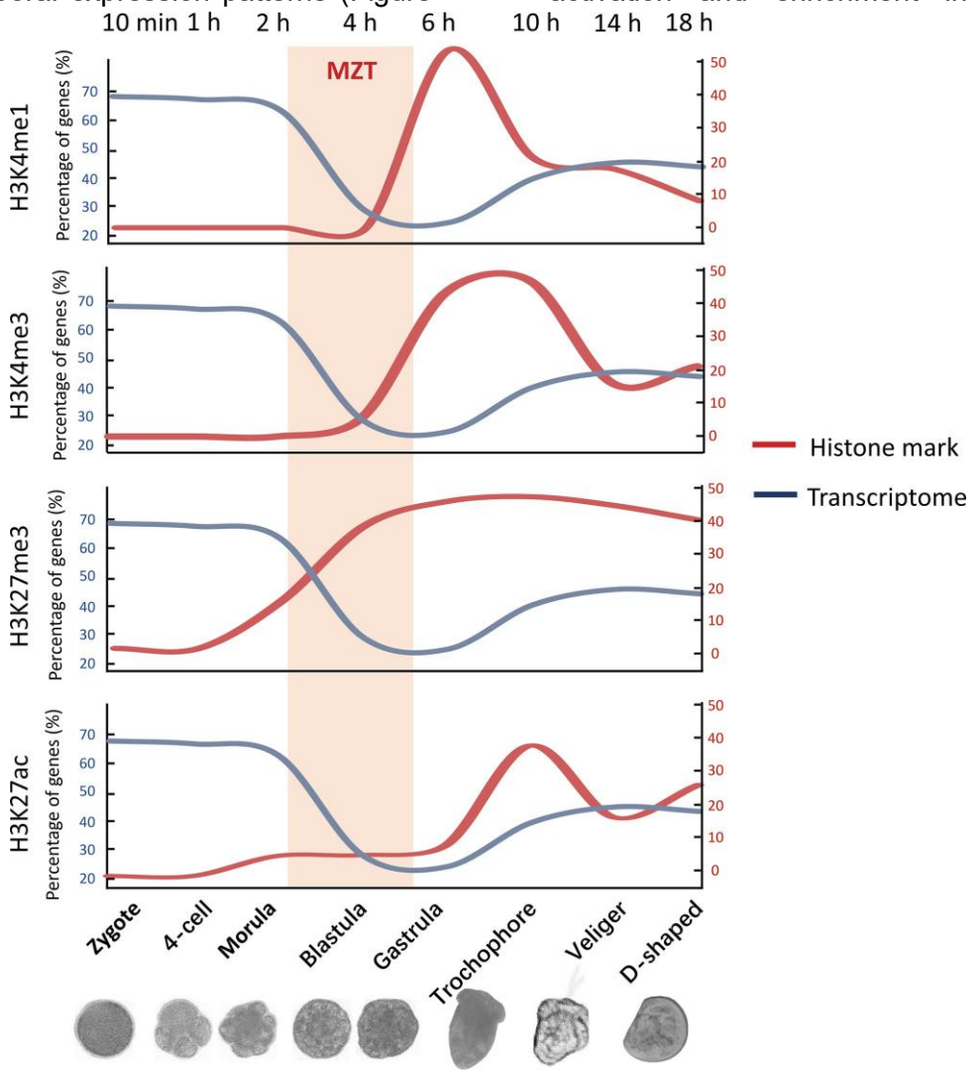

Figure 4 Dynamic model of histone modification changes and transcriptional activity during early embryonic development in *Mulinia lateralis*

keeping things stable (Fellous et al., 2019). These findings imply that chromatin states are formed sooner and stay rather stable in C. gigas in contrast to M. Lateralis. The scallop (Patinopecten yessoensis), on the other hand, exhibits significant histone demethylation across all developmental stages, suggesting ongoing chromatin remodeling (Guo et al., 2020). Since the current work used CUT&Tag, which offers higher-resolution insights into chromatin state transitions, while previous studies used global methylation tests, these interspecies variances may be the result of different developmental tactics or methodological variations. Table 1 summarizes the timing of ZGA and associated histone modification patterns among a few chosen species to make cross-species comparisons easier.
When combined, the dynamics of histone modification shown in
The M. lateralis that are most similar to those found in Drosophila, with minimal histone signals before ZGA and the gradual formation of permissive (H3K4me1, H3K4me3, and H3K27ac) and repressive (H3K27me3) marks after genome activation. Interestingly, H3K27me3's quicker and wider establishment in comparison to activating alterations might be a unique regulatory characteristic in

The M. lateralis, which would indicate a chromatin priming technique unique to a lineage.

RECOMMENDATIONS

The dynamics of histone modifications and transcriptome reprogramming during M are thoroughly examined in this work. lateralis embryogenesis, clarifying important regulatory aspects related to ZGA and developmental advancement. Prior to the extensive accumulation of permissive modifications like H3K4me3, H3K27ac, and H3K4me1, H3K27me3 became a widely recognized repressive chromatin mark that was deposited early in development, most likely mediated by EZH2-containing PRC2. The spatiotemporal synchronization of embryonic gene activation across several cell lineages during later embryogenesis may be facilitated by these early-deposited histone changes. While integrative analysis of actively transcribing genes showed enrichment in important developmental signaling pathways, such as Hippo, WNT, MAPK, and biomineralization, chromatin state profiling made it possible to identify cis-regulatory elements. Key players in lineage specification and morphogenesis, including yap1, ppp2r1b, mtor, and smad4, were identified as transcriptionally active at particular phases. These results provide M with a fundamental epigenomic framework. lateralis, promoting bivalve developmental genomics and supporting more general uses in aquaculture and evolutionary epigenetics.
To determine the causal roles of histone modifications in early development, future research should include functional validation using targeted perturbation techniques like CRISPR-mediated editing, single-cell epigenomic profiling (e.g., single-cell CUT&Tag, ATAC-seq), and chromatin accessibility assays. The evolutionary variability of chromatin control in marine invertebrates will be better understood by cross-species comparative investigations. This study establishes M by combining genome-wide epigenetics with molecular developmental biology. lateralis as a useful model for researching the evolution of cis-regulatory architecture and histone modification reprogramming in marine species that are not models.

AVAILABLE DATA

The CUT&Tag and RNA-seq data produced in this study have been uploaded to the Science Data Bank (CSTR:31253.11.sciencedb.j00139.00244 for RNA-seq data and CSTR:31253.11.sciencedb.j00139.00243 for CUT&Tag data), the NCBI database (BioProjectID PRJNA1224210 and PRJNA1257552), and the Genome Sequence Archive in National Genomics Data Center, China National Center for Bioinformation/Beijing Institute of Genomics, Chinese Academy of Sciences (https://ngdc.cncb.ac.cn/gsa) under accession numbers CRA045750 and CRA045756. You can obtain the additional file with the chromHMM output files from figshare at

https://doi.org/10.6084/m9.figshare.28418309.v2.

ADDITIONAL INFORMATION

This article's supporting information is available online.

Rival Interests

There are no conflicting interests, according to the authors.

THE WORKS OF THE AUTHORS

Z.Y. and the study was conceived by J.L.S. Z.M.B., J.J.H., and Z.Y. oversaw the research. Z.Y. and the experiments were designed by J.L.S. The experiments were carried out by J.L.S. and M.M.Y. The data analysis and visualization were carried out by J.L.S., J.X.L., and Z.C.W. Technical assistance was given by Z.J.Y. Funding assistance was provided by Z.Y., J.J.H., and Z.M.B. Z.Y. and the draft manuscript was written by J.L.S. The completed manuscript was read and approved by all authors.

THANK YOU

For this study, we are grateful to the Ocean University of China's High-Performance Biological Supercomputing Center.

RESOURCES

Lesch BJ, Bae S. 2020. Transcription status and poising at promoters are predicted by the distribution of H3K4me1. Cell and Developmental Biology Frontiers, 8: 289.

Kouzarides T., Bannister AJ. 2011. Histone alterations control the chromatin. 21(3), Cell Research, 381–395.

Nešić S, Vićić I, Banović Đeri B, et al. 2024. Five NGS mapping techniques are benchmarked for the reference alignment of short RNAs linked to bacterial outer membrane vesicles. Microbiological Frontiers, 15: 1401985.

Kabbe M, Castelo-Branco G, Bartosovic M. 2021. In complicated tissues, single-cell CUT&Tag examines transcription factors and histone alterations. 39(7), Nature Biotechnology, 825–835.

Love JC, Shapovalova Y, Beadle LF, et al. 2023. P-bodies are implicated in 5′ to 3′ degradation, according to a combination of single-molecule imaging in the Drosophila embryo and modeling of mRNA decay dynamics. e3001956 in PLoS Biology, 21(1).

Francis H, Rampasekova A, Blayney JW, et al. 2023. Classical enhancers and facilitators that completely activate gene expression are examples of super-enhancers. 186(26): 5826–5839; Cell. E18.

Blelloch R, Chen KX, Boileau RM. 2023. During the development of embryonic stem cells, loss of MLL3/4 separates enhancer H3K4 monomethylation, H3K27 acetylation, and gene activation. 24(1), Genome Biology: 41.

Bolar NA, Živná M, Golzio C, et al. (2016). Autosomal-dominant tubulo-interstitial and glomerulocystic kidney disease with anemia is caused by heterozygous loss-of-function SEC61A1 mutations. 174–187 in The American Journal of Human Genetics, 99(1).

Henikoff S, Brahma S. 2024. To remove nucleosomes, the BAF chromatin remodeler works in concert with transcription factors and RNA polymerase II. 56(1), Nature Genetics, 100–111.

Padamsi Z, Fakim H, Brandmann T, et al. 2018. The molecular makeup of interactions with LSM14 that contribute to the formation of mRNA silencing complexes. e97869 in The EMBO Journal, 37(17).

Bianchi N, Džafo E, Chirichella M, et al. 2022. The miR-150/PDAP1 axis, which is regulated by RFX transcription factors, limits the growth of human T cells. e3001538 in PLoS Biology, 20(2).

Atinbayeva N, Pane A, Ciabrelli F, et al. 2024. Regulation of gene expression and epigenetic inheritance in early Drosophila embryos. Reports on EMBO, 25(10): 4131–4152.

Blanco M, Crespo M, Damont A, et al. 2020. A unique signature at the promoters and distal enhancers of active genes is revealed by multi-omic study of gametogenesis. Research on Nucleic Acids, 48(8): 4115–4138.

Schlesinger F, Davis CA, Dobin A, et al. (2013). STAR is an ultrafast universal RNA-seq aligner. 29(1), Bioinformatics, 15–21.

Lebedev E, Adonin L, Drozdov A. 2023. Examining the dichotomy in Bilateria through a comparative study of sea urchin and bivalve genetics and development. Molecular Sciences International, 24(24): 17163.

Goll MG, Artis AR, and Duval KL. 2024. the changing chromatin landscape of H3K9me3 in zebrafish embryos. iyae138 in Genetics, 228(2).

Schmitz RJ, Springer NM, Eichten SR. 2014. Beyond chromatin changes and intricate genetic regulation is epigenetics. 933–947 in Plant Physiology, 165(3).
Kellis M., Ernst J. 2017. ChromHMM is used for genome annotation and chromatin-state finding. 2478–2492 in Nature Protocols, 12(12).
Luquet E, David P, Fallet M, et al. 2020. Mollusks' intergenerational impacts and epigenetic inheritance. Gene, 729: 144166.
Le Franc L, Jouaux A, Fellous A, et al. 2019. In the early stages of the Pacific oyster Crassostrea gigas' development, histone methylation plays a role in controlling gene expression. Genes, 10(9): 695.
Liu T, Qin B, Feng JX, et al. (2012). ChIP-seq enrichment detection with MACS. 1728–1740 in Nature Protocols, 7(9).
United Nations Food and Agriculture Organization (FAO). 2024. The situation of nutrition and food security worldwide in 2024: funding to eradicate all types of malnutrition, hunger, and food insecurity. FAO Report, Rome, 246.
Takeda H, Fukushima HS, and Nakamura R. 2023. Histone markers are not completely erased during epigenetic reprogramming in the early stages of medaka growth. 33(4): 572–586, Genome Research.
Li XX, Zhao F, Guo XL, et al. 2023. Full-length transcriptome research sheds light on Mulinia lateralis larval shell development. Marine Science Frontiers, 9: 1111241.
Zhang LJ, Li YJ, Guo ZY, et al. 2020. Histone demethylation may have a role in controlling early development and gametogenesis, according to expression profiling of the Kdm genes in scallop Patinopecten yessoensis. Part B: Biochemistry and Molecular Biology, Comparative Biochemistry and Physiology, 243–244: 110434.
Belton C, Hanna CW, Huang JH, et al. 2022. Genomic histone 3 lysine 4 trimethylation is redistributed when histone methyltransferase SETD1B is lost during oogenesis. Research on Nucleic Acids, 50(4): 1993–2004.
Wike CL, Nie XC, Hickey GJ, et al. 2022. recruitment of an organized polycomb complex in early zebrafish embryos to establish developmental gene silencing. eLife, 11: e67738.
Csankovszki G, Jash E. 2024. arrangement of chromatin during C. Elegans early stages of development. 4(1): 64–83; DNA.
Liu X, Jiao LY. 2015. Histone H3K27 trimethylation by an active polycomb repressive complex 2: structural underpinnings. Science, 350 (6258): aac4383.
Henikoff JG, Janssens DH, Kaya-Okur HS, et al. 2020. economical and effective chromatin profiling with CUT&Tag. 15(10), Nature Protocols, 3264–3283.
Wu SJ, Codomo CA, Kaya-Okur HS, et al. 2019. For effective epigenomic profiling of single cells and tiny samples, use CUT&Tag. 1930 in Nature Communications, 10(1).
Anastassiadis K, Kranz A. 2020. SETD1A and SETD1B's functions in sickness and development. Gene Regulatory Mechanisms, Biochimica et Biophysica Acta (BBA), 1863(8): 194578.
P. Langfelder and S. Horvath. 2008. WGCNA is a weighted correlation network analysis program for R. 559 in BMC Bioinformatics, 9(1).
Courtney AJ, Laue K, Rajshekar S, et al. 2019. The zebrafish embryo's genome-wide heterochromatin formation is controlled by the maternal to zygotic transition. 1551 in Nature Communications, 10(1).
Huber W, Lawrence M, Pagès H, et al. (2013). Genomic range computation and annotation software. e1003118 in PLoS Computational Biology, 9(8). Bork P., Letunic I. 2021. An online tool for displaying and annotating phylogenetic trees is called Interactive Tree of Life (iTOL) v5. Research on Nucleic Acids, 49(W1): W293–W296.
Li H. 2013. using BWA-MEM to align assembly contigs, clone sequences, and sequence reads. https://doi.org/10.48550/arXiv.1303 is the doi for arXiv. 3997
Durbin R, Li H. 2009. Using the Burrows-Wheeler transform, short read alignment is quick and precise. 1754–1760 in Bioinformatics, 25(14).
Shi W, Smyth GK, and Liao Y. 2014. An effective general-purpose application for allocating sequence reads to genomic features is featureCounts. 30(7), Bioinformatics, 923–930.
Reiner AH, Lindeman LC, Andersen IS, et al. 2011. Before the zygotic genome is activated, altered histones prepare the expression of

developmental genes. 21(6), Developmental Cell, 993–1004.
Zimmermann R, Schick B, and Linxweiler M. 2017. In signal transduction, cancer, and personalized medicine, let's discuss Secs. 61, 62, and 63. Targeted Therapy and Signal Transduction, 2(1): 17002.
He YL, Wu XT, Liu BF, et al. 2024. TCF3/12 is identified as a crucial regulator of folliculogenesis by mapping putative enhancers in mouse oocytes and early embryos. 962–974 in Nature Cell Biology, 26(6).
Liu BZ, Liu G, and Huan P. 2014. Two Smad genes' cloning and expression patterns during the Pacific oyster Crassostrea gigas's embryonic development and shell production. 32(6), 1224–1231, Chinese Journal of Oceanology and Limnology.
Huber W, Anders S, Love MI. 2014. DESeq2-based moderated estimation of fold change and dispersion for RNA-seq data. 550 in Genome Biology, 15(12).
Zhuang XW, Lu T, and Ang CE. 2022. Epigenomic profiling of individual cells in complex tissues with spatial resolution. 185(23): 4448–4464; Cell. E17.
Haccard O, Chesneau A, Meléndez García R, et al. 2022. Yap has a non-transcriptional role in controlling Xenopus laevis's DNA replication program. eLife, 11: e75741.
Bannister AJ, Burton A, Millán-Zambrano G, et al. 2022. Post-translational changes in histones: their cause and effect on genome function. 563–580 in Nature Reviews Genetics, 23(9).
Jain M, Patel RK. 2012. The NGS QC Toolkit is a collection of tools for ensuring the quality of results from next-generation sequencing. e30619 in PLoS One, 7(2).
Torres-Padilla ME, Pecori F. 2023. Nuclear architecture dynamics in the early stages of embryonic development: insights from live imaging. 435–449 in Developmental Cell, 58(6).
Zacarias-Cabeza J, Benoukraf T, Pekowska A, et al. (2011). The epigenetic hallmark of activated enhancers is provided by H3K4 trimethylation. Journal of EMBO, 30(20): 4198–4210.
Pinello L, Orkin SH, Xu J, et al. (2014). Cell-type-specific regulators of H3K27me3 patterns are identified using chromatin-state plasticity analysis. United States of America: Proceedings of the National Academy of Sciences, 111(3): E344–E353.
Quinlan AR. 2014. The Swiss-Army tool for analyzing genomic features is called BEDTools. Bioinformatics Current Protocols, 47: 11.12. 1–11.12. 34.
Garduño RA, Rivera-Casas C, Gonzalez-Romero R, et al. (2017). Biochemical and molecular techniques that are helpful for the epigenetic description of

Bivalve molluscs' chromatin-associated proteins. The boundaries of physiology, 8: 490.
Kundaje A, Meuleman W, Roadmap Epigenomics Consortium, et al. (2015). 111 reference human epigenomes were analyzed holistically. 317–330 in Nature, 518(7539).
Bork P, Schultz J, Milpetz F, et al. 1998. SMART is a straightforward modular architecture research tool for identifying signaling domains. 95(11): 5857–5864, Proceedings of the National Academy of Sciences of the United States of America.
Harrison MM, Schulz KN. 2019. mechanisms that control the activation of the zygotic genome. 221–234 in Nature Reviews Genetics, 20(4).
Datta K, Pandey P, Seshacharyulu P, et al. (2013). Phosphatase: The structural significance, control, and abnormal expression of PP2A in cancer. 335(1), Cancer Letters, 9–18.
Li M, Shen MH, Di GL, et al. (2018). Proteomics research on Babylonia areolata's three larval developmental stages and transformations. 8(1): 6269 in Scientific Reports.
Castillo-Aleman YM, Iglesias-Barrameda N, Sotomayor-Lugo F, et al. 2024. Histone modification kinetics during zygotic genome activation in mammals. Journal of Molecular Sciences International, 25(3): 1459.
Haggerty C, Luo EC, Stefano BD, et al. 2019. By altering P-body homeostasis, the RNA helicase DDX6 regulates cellular plasticity. 25(5), Cell Stem Cell, 622–638. E13.
Chen GR, Eichhorn SW, Subtelny AO, et al. (2014). An embryonic shift in translational control is shown by poly(A)-tail profiling. Nature, 508 (7494), 66–71.
Li XF, Luo H, Sun L, et al. 2023. Endothelial dysfunction can be inhibited by EZH2 as a therapeutic drug. Pharmacological Biochemistry, 213: 115594.

Stecher G, Kumar S, Tamura K. 2021. Molecular evolutionary genetics analysis version 11, or MEGA11. 38(7): 3022–3027; Molecular Biology and Evolution.
Gambello MJ, Toyo-oka K, Shionoya A, et al. 2003. By binding to NUDEL, 14-3-3ε plays a crucial role in neuronal migration, providing a mechanistic explanation for Miller-Dieker syndrome. 34(3), Nature Genetics, 274–285.
Turner, BM. 2007. An epigenetic code definition. 9(1): 2–6 in Nature Cell Biology.
Lipshitz HD, Vastenhouw NL, and Cao WX. 2019. The passage from mother to zygote is reviewed. Dev161471, Development, 146(11).
Hoellein TJ, Vaughn CC. 2018. bivalve effects on marine and freshwater environments. Ecology, Evolution, and Systematics Annual Review, 49: 183–208.
Raby L, Bary A, Völkel P, et al. 2019. Zebrafish development does not require the function of Ezh1, which results from the duplication of the Ezh2 gene. 9(1): 4319 in Scientific Reports.
Liu XY, Wang CF, Chen C, et al. 2022. Following fertilization, dynamic nucleosome organization identifies regulatory elements for the activation of the mouse zygotic genome. 32(9), Cell Research, 801–813.
Zhang LL, Wang J, Lian SS, et al. 2020. A single intercalation genesis of metazoan larvae is supported by evolutionary transcriptomics of the biphasic life cycle. Ecology & Evolution in Nature, 4(5): 725–736.
Linke M, Hengstschätger M, and Weichhart T. 2015. mTOR controls the activity of innate immune cells. Immunology in Nature Reviews, 15(10): 599–614.
Wickham, H. 2011. Ggplot2. Computational Statistics in WIREs, 3(2):

180–185.
Fan DD, Zhao H, Wu KL, et al. 2023. Histone acetylation dynamics in the early stages of human embryogenesis. 29 in Cell Discovery, 9(1).
Mihalas AB, Wu SJ, Furlan SN, et al. 2021. CUT&Tag study of chromatin changes in tumor growth and differentiation in single cells. Nature Biotechnology, 39(7), 819–824.
Wu X, Zhao HY, Heffelfinger C, et al. 2019. Finding plant variety using benchmarking variant identification systems. Genes, BMC, 20(1): 701. Yu G, Xia WK, Xu JW, et al. 2019. Histone changes are reset during the human parental-to-zygotic transition. 353–360 in Science, 365(6451).
Li C, Liu XY, Xu RM, et al. 2021. insights into early mammalian embryonic epigenetic processes. Protein & Cell, 12(1): 7–28.
Shen WL, Yang J, Liu MH, et al. 2022. The epigenetic regulatory landscape in the gill tissue of the giant yellow croaker (Larimichthys crocea) under low salinity stress is revealed by H3K4me3 CUT&Tag and transcriptome analysis. Marine Science Frontiers, 9: 906337.
Yang ZJ, Wang H, Huang XT, and others (2021). Effects of microalgae diets and stocking density on larval growth, survival and metamorphosis of dwarf surfclam, Mulinia lateralis. 736440 in Aquaculture, 536.
Ye Z, Braden CR, Wills A, et al. 2021. Identification of in vivo Hox13-binding sites reveals an essential locus controlling zebrafish brachyury expression. Development, 148(11): dev199408.
Yu GC, Wang LG, Han YY, et al. 2012. clusterProfiler: an R package for comparing biological themes among gene clusters. OMICS: A Journal of Integrative Biology, 16(5): 284–287.
Yu GC, Wang LG, He QY. 2015. ChIPseeker: an R/Bioconductor package for ChIP peak annotation, comparison and visualization. Bioinformatics, 31(14): 2382–2383.
Yu Y, Li XJ, Jiao R, et al. 2023. H3K27me3-H3K4me1 transition at bivalent promoters instructs lineage specification in development. Cell & Bioscience, 13(1): 66.
Zenk F, Loeser E, Schiavo R, et al. 2017. Germ line-inherited H3K27me3 restricts enhancer function during maternal-to-zygotic transition. Science, 357(6347): 212–216.
Zhang BJ, Wu XT, Zhang WH, et al. 2018. Widespread enhancer dememorization and promoter priming during parental-to-zygotic transition. Molecular Cell, 72(4): 673–686. e6.
Zhang W, Liu HT. 2002. MAPK signal pathways in the regulation of cell proliferation in mammalian cells. Cell Research, 12(1): 9–18.
Zhao M, Shi Y, He MX, et al. 2016. PfSMAD4 plays a role in biomineralization and can transduce bone morphogenetic protein-2 signals in the pearl oyster Pinctada fucata. BMC

Developmental Biology, 16(1): 9. Zheng QW, Wu XT, Li X, et al. 2024. Low-input CUT&Tag for efficient epigenomic profiling of zebrafish stage I oocytes. Frontiers in Cell and Developmental Biology, 12: 1475912.
Zhu W, Xu XC, Wang XX, et al. 2019. Reprogramming histone modification patterns to coordinate gene expression in early zebrafish embryos. BMC Genomics, 20(1): 248.
Zhu Y, Li WN, Dong YF, et al. 2023. C. elegans hemidesmosomes sense collagen damage to trigger innate immune response in the epidermis. Cells, 12(18): 2223.
Zinski J, Tajer B, Mullins MC. 2018. TGF-β family signaling in early vertebrate development. Cold Spring Harbor Perspectives in Biology, 10(6): a033274.